

Promising electrochemical performance of high-surface-area boron-doped diamond/carbon nanotube electroanalytical sensors

Bruna C. Lourencao¹ · Tiago A. Silva¹ · Hudson Zanin² · Paul W. May³ · Evaldo J. Corat⁴ · Orlando Fatibello-Filho¹

Received: 8 October 2015 / Revised: 14 January 2016 / Accepted: 17 January 2016
© Springer-Verlag Berlin Heidelberg 2016

Abstract Porous boron-doped diamond (p-BDD) electrodes of high-surface-area have been prepared on vertically aligned carbon nanotube substrates, and their electrochemical performance has demonstrated promising results for application in electroanalysis. The electrochemical features of the p-BDD electrodes were investigated and compared with those of a conventional flat BDD electrode (f-BDD). From cyclic voltammetry studies performed for the electrochemical probes $[\text{Fe}(\text{CN})_6]^{3-}$ and *N,N,N',N'*-tetramethyl-*para*-phenylenediamine (TMPD), a fast charge transfer was observed at the p-BDD/electrolyte interface. For the $[\text{Fe}(\text{CN})_6]^{3-}$ redox probe, the heterogeneous electron-transfer rate constant (k^0) value obtained for p-BDD was 10.9 times higher than that obtained using a f-BDD electrode. Moreover, the p-BDD electrodes also gave a smaller peak potential separation, ΔE_p , and larger analytical signal magnitude for different biomolecules, such as dopamine (DA), acetaminophen (AC), and epinephrine (EP). These set of results

demonstrated that the p-BDD electrode is a suitable candidate for applications in electroanalytical chemistry.

Keywords Porous boron-doped diamond · Electroanalytical application · Dopamine · Acetaminophen · Epinephrine

Introduction

Carbon electrodes, in general, are widely used both in electrochemical and in electroanalytical applications since they possess very interesting mechanical properties, a wide potential window, chemical inertness, and versatility for surface modifications. There are many types of carbonaceous materials that are used as electrodes; among these are glassy carbon, pyrolytic carbon, carbon paste, graphite, boron-doped diamond (BDD), and carbon nanotubes. However, in recent years, new types of carbon materials such as graphene [1], and also hybrid materials of carbon such as boron-doped graphene [2] and graphene-carbon nanotubes [3], have been used as working electrodes and have drawn attention because of their excellent performance.

Conventional flat BDD (f-BDD) electrodes have a large number of electrochemical properties distinguishable from other commonly used carbonaceous electrodes which are very attractive for electrochemical studies, such as low background current, extreme electrochemical stability in both alkaline and acidic media, high response sensitivity, good resistance to fouling, and a wide working potential window in aqueous solutions [4–9]. Moreover, different structures, shapes, and sizes of the BDD electrode surfaces can show different electrochemical features [10–13]. Higher sensitivity and improved selectivity of structure-modified BDD compared with f-BDD electrodes have been reported [14]. Luo et

✉ Bruna C. Lourencao
brunalourencao@gmail.com

✉ Hudson Zanin
hudsonzanin@gmail.com

¹ Department of Chemistry, São Carlos Federal University, P. O. Box 676, São Carlos, SP CEP: 13560-970, Brazil

² Laboratory of Energy Storage & Supply (ES&S), Institute of Research and Development (IP&D), Univap, Av. Shishima Hifumi 2911, São José dos Campos, SP CEP: 12224-000, Brazil

³ School of Chemistry, University of Bristol, Cantock's Close, Bristol BS8 1TS, UK

⁴ National Institute for Space Research, Avenida dos Astronautas 1758, São José dos Campos, SP CEP: 12227-010, Brazil

al. [10] reported the fabrication and characterization of a BDD nanorod forest (BDDNF) electrode and the study of its electrochemical applicability in nonenzymatic amperometric detection of glucose. They prepared the BDDNF on silicon nanowires (SiNWs), turning an f-BDD electrode into a three-dimensional structured diamond electrode. According to the authors, this BDDNF electrode exhibited very attractive electrochemical performance compared to f-BDD electrodes, notably improved sensitivity and selectivity for biomolecule detection.

The electrochemical behaviour of different redox systems and detection of catechol were investigated on f-BDD electrodes and “nanograss array BDD” by Lv et al. [11]. When compared with f-BDD, the nanograss array BDD presented an improvement in relation to reactive site, electron transfer, as well as promoting electrocatalytic activity and enhancing selectivity.

Porous boron-doped diamond (p-BDD) films are considered a novel class of carbon hybrid materials that also has interesting characteristics for use in electroanalysis. These materials show great promise as sensitive and high-surface-area electrodes [15, 16]. To produce the p-BDD films, vertically aligned carbon nanotubes (VACNT) were used as scaffolds. The VACNT were first seeded with a suspension of nanodiamonds in liquid (water or methanol) causing the CNTs to stick together at their tips. Depending upon the length and areal density of the CNTs, when stuck together they formed a variety of 3D microstructures, including teepees [17] and honeycombs or ridges [15]. Careful deposition of diamond by chemical vapour deposition (CVD) onto these structures permanently fixed the structure into shape by enclosing it in a thin (<1 μm) layer of polycrystalline diamond. Addition of diborane to the CVD process ensured that the diamond coating was B-doped and, hence, exhibited near-metallic conductivity. These 3D microstructures combined the excellent conductivity and electron transport of carbon nanotubes (CNTs) [18] with the desirable electrochemical properties of BDD, such as chemical stability and large potential window [5].

According to Corat et al. [15], the surface area of these new porous BDD electrodes is much higher than those found in f-BDD electrodes. This is due to it having a morphology similar to ridges, which significantly extends the chemically active area—a desirable feature for electroanalytical applications, for example. These properties make the p-BDD electrodes a promising material for use as sensors or energy storage devices [15, 16, 19–22] as well as suitable candidates for application in electroanalytical chemistry. Thus, in the present work, we have explored for the first time the performance of p-BDD films as an electrochemical sensor for different redox probes and important biomolecules.

Experimental

Material synthesis

p-BDD films were prepared using VACNTs as scaffolds as previously reported [15, 23, 24]. Briefly, a 10-nm Ni layer was deposited on a Ti substrate by e-beam evaporation and placed into a 2.45-GHz microwave (MW) plasma CVD chamber. A N_2/H_2 (10/80 sccm) plasma was used to heat the substrate, causing the thin Ni layer to ball up into nanoparticles that became the catalyst particles for subsequent VACNT growth in the same chamber. The length, diameter, and areal density of the CNTs could be varied by changing the growth conditions. For the CNTs reported here, CH_4 (12 sccm) was the process gas which was introduced into the chamber for 1 min, maintaining a substrate temperature of 760 $^\circ\text{C}$ and a reactor pressure of 30 Torr. This produced a VACNT forest of CNTs with length $\sim 20 \mu\text{m}$, width $\sim 20\text{--}50 \text{ nm}$, and areal density of $\sim 10^{10} \text{ cm}^{-2}$. Electrospray seeding of nanodiamonds [25] followed by diamond CVD was then performed for 0.5 h using a hot filament reactor and 2 % CH_4/H_2 with diborane (B_2H_6) as a source of boron. The gas-phase B concentration was sufficient to ensure that the diamond was heavily doped and therefore had near-metallic conductivity. As a control sample, a BDD film was deposited onto a flat single-crystal (100) Si substrate (p+, resistivity 0.01–0.02 $\Omega \text{ cm}$) using the same CVD conditions except for a deposition time of 7 h.

Electrochemical assays

A conventional three-electrode cell was used for the electrochemical assays, with an Ag/AgCl (3.0 mol L^{-1} KCl) reference electrode, a Pt foil as counter electrode, and the p-BDD or f-BDD electrode as the working electrode. The geometric areas of the p-BDD and f-BDD were 0.64 and 0.35 cm^2 , respectively. A potentiostat/galvanostat $\mu\text{Autolab}$ type III (Ecochemie) controlled with GPES software (version 4.9) was employed for the electrochemical measurements.

Cyclic voltammetry (CV) was used to assess the electrochemical performance of the p-BDD electrodes for the response of two soluble redox probes, $[\text{Fe}(\text{CN})_6]^{3-}$ and *N,N,N',N'*-tetramethyl-*p*-phenylenediamine (TMPD) in 0.1 mol L^{-1} KCl. Electrochemical impedance spectroscopy (EIS) measurements were carried out over a frequency range of 100 kHz–0.01 Hz and amplitude of 10 mV. All chemicals were purchased from Sigma-Aldrich.

The electrochemical performance of the p-BDD electrode was also evaluated for the important biomolecules of known redox behaviour, dopamine (DA), acetaminophen (or paracetamol) (AC), and epinephrine (or adrenaline) (EP) by CV. All the CV experiments for DA, EP, and AC were conducted in a 0.2 mol L^{-1} phosphate buffer solution at pH 7.0. CVs were

collected in the potential scan rate range from 10 to 500 mV s⁻¹ at a fixed analyte concentration of 1.0 mmol L⁻¹.

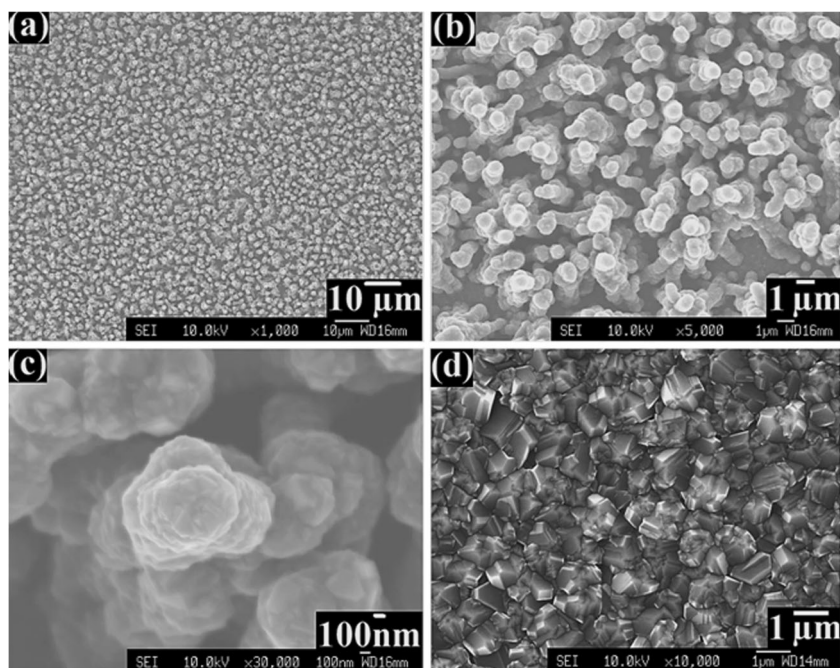
Results and discussion

Material characterization and electrochemical properties

Figure 1a–d consists of SEM micrographs obtained for the porous and flat BDD surfaces. Analyzing the SEM images collected for the p-BDD (Fig. 1a–c) confirms that the VACNTs were completely covered by the BDD coating. In addition, for the preparation of the p-BDD samples, VACNTs with 20 μm length and areal density ~10¹⁰ cm⁻² were employed as a substrate. Using these VACNTs, the diamond-coated CNTs form ridge-like structures, and each ridge contains ~200 CNTs, although this varies depending on the amount of lateral interconnection between ridges. A continuous microcrystalline BDD film with a thickness of ~1–2 μm was obtained in the flat BDD case, with a surface morphology as shown in Fig. 1d. Raman spectra of p-BDD and f-BDD (data not shown, please see both Fig. 2 of references [15, 26] and Fig. 3 of reference [24]) showed the typical peak for sp³ diamond at 1332 cm⁻¹ and sp² bands (D ~1350 cm⁻¹ and G between 1550 and 1600 cm⁻¹). Consequently, the p-BDD sample is a combination of both diamond and carbon nanotube structural characteristics and, therefore, it is expected that the obtained composite may combine the electrochemical properties of both carbon materials.

Initially, the behaviour of both BDD electrodes was evaluated in 0.1 mol L⁻¹ KCl solution at 50 mV s⁻¹ in the potential range from -0.2 to +0.6 V. In Fig. 2, the cyclic voltammograms obtained using the f-BDD and p-BDD electrodes in the KCl solution are shown. A considerable increase in capacitive current was observed for the p-BDD electrode. The capacitive (background) current measured only in the supporting electrolyte solution suggests a higher double-layer capacitance and surface area for the p-BDD electrode consistent with the SEM images. To quantify the double-layer capacitance, CV measurements were recorded at different potential scan rates ($v = 10\text{--}500\text{ mV s}^{-1}$) in the same supporting electrolyte solution. The relationship $C = \Delta j/2v$ [27] was used to determine C , the double-layer capacitance, with Δj being the difference between the anodic and cathodic current densities at 0.25 V. Figure 3a shows the CVs recorded for different potential scan rates for the p-BDD electrode. The relationship between Δj and v was linear, as expected, with the respective slope equal to $2C$ (see inset of Fig. 3a). Thus, C for the p-BDD and f-BDD electrodes was 327 and 0.96 μF cm⁻², respectively. The C values recorded for the f-BDD electrode is in accordance with the typical double-layer capacitance results obtained for standard BDD electrodes, such as those proposed by Swain and collaborators (ranging from 1.0 to 3.0 μF cm⁻² depending on the supporting electrolyte solution pH) [28, 29]. It follows that the double-layer capacitance for the p-BDD electrode was approximately 340 times higher than that for the f-BDD electrode, which is consistent with the larger surface area of the p-BDD electrodes.

Fig. 1 SEM micrographs of as-grown (a–c) p-BDD and (d) f-BDD films



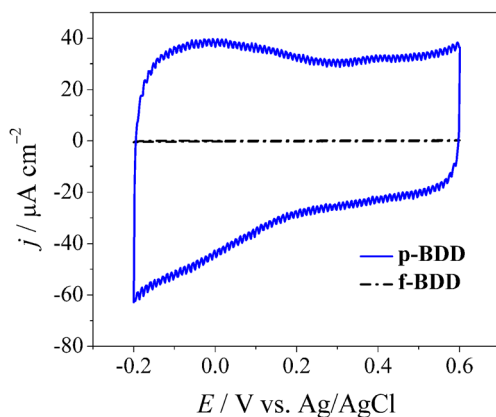


Fig. 2 CVs obtained in 0.1 mol L⁻¹ KCl solution at 50 mV s⁻¹ using the p-BDD and f-BDD electrodes

EIS measurements were also performed using a 0.1 mol L⁻¹ KCl solution as supporting electrolyte. The Bode plots for both electrodes are shown in Fig. 3b. For an example frequency of 0.1 Hz, the modulus of the impedance (Z) for p-BDD is ~ 33 times lower than that for f-BDD. Additionally, analysing the EIS spectra for redox probe $[\text{Fe}(\text{CN})_6]^{3-}$ in 0.1 mol L⁻¹ KCl solution (data not shown), it was observed a well-defined semi-circle at higher frequencies when f-BDD was used, which decrease considerably using p-BDD. This behaviour revealed that the electron-transfer resistance decreased dramatically when p-BDD was used, which demonstrate the improvement of the heterogeneous electron-transfer kinetics on the electrode surface in agreement with results showed on Fig. 3.

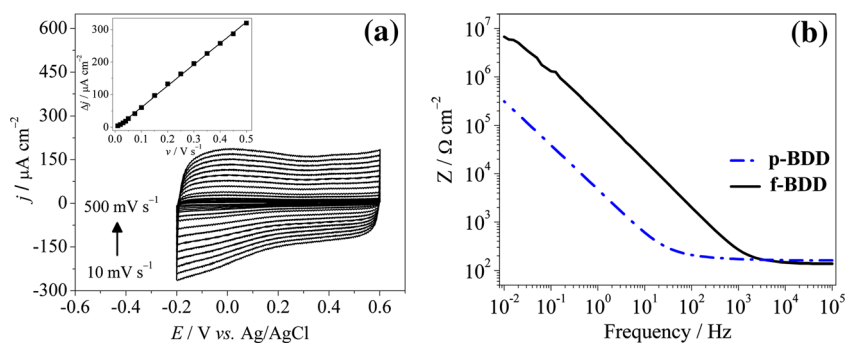
One important parameter to assess the quality of an electrode material is the heterogeneous electron-transfer rate constant (k^0), which is intrinsically associated with the ΔE_p values, where a smaller ΔE_p value represents an increased reversibility and faster heterogeneous electron-transfer kinetics at a given electrode material [30]. The response to a redox probe, such as hexacyanoferrate (III) ($[\text{Fe}(\text{CN})_6]^{3-}$) [31], is commonly used to evaluate k^0 between an electrode and electroactive species present in solution. The k^0 value is

strongly influenced by several variables, such as the electronic properties and the surface chemistry (e.g., surface terminations and the surface cleanliness) of the electrode [32]. Typical CVs for both electrodes at a potential scan rate of 50 mV s⁻¹ (Fig. 4a) show a well-defined pair of redox peaks with a peak potential separation (ΔE_p) of ~ 79 and 149 mV for p-BDD and f-BDD, respectively. The p-BDD presents a smaller ΔE_p value than f-BDD, which suggests a more favourable electrochemical interaction at the electrode surface and, thus, enhanced electron-transfer kinetics.

In order to calculate the k^0 values for p-BDD and f-BDD electrodes, CV assays at different potential scan rates (10–500 mV s⁻¹) were performed. In Fig. 4b, the CVs obtained for a 1.0×10^{-3} mol L⁻¹ $[\text{Fe}(\text{CN})_6]^{3-}$ solution in 0.1 mol L⁻¹ KCl at different potential scan rates using the p-BDD electrode are shown. The voltammetric peak currents (anodic, I_{pa} , and cathodic, I_{pc}) were monitored as a function of potential scan rate (v). In each case, the plots of I_p versus $v^{1/2}$ were linear, indicating diffusional processes dominate (inset (i) in Fig. 4b). Moreover, linear relationships between the logarithm of peak current ($\log I_p$) and the logarithm of potential scan rate ($\log v$) were obtained, with slopes of 0.45 (for anodic peak current) and 0.44 (for cathodic peak current), which are close to the theoretical value of 0.5 found for an electroodic process governed by diffusion. Thus, the Nicholson [33] method was applied to estimate the k^0 values. No correction was made for uncompensated ohmic drop (iR) effects. Therefore, we determined the k^0 values as apparent rate constants, k^0_{app} with values of 9.2×10^{-3} and 1.4×10^{-3} cm s⁻¹ for p-BDD and f-BDD, being obtained, respectively, using a diffusion coefficient (D) of 6.2×10^{-6} cm² s⁻¹ for $[\text{Fe}(\text{CN})_6]^{3-}$ in 0.1 mol L⁻¹ KCl. Comparing these k^0_{app} values, the result for p-BDD is 6.6 times higher than that for f-BDD, indicating a significant improvement in the electron-transfer rate on the p-BDD surface. This can be related to the higher electrical conductivity (or the reduction of the electrical resistivity) provided by the VACNT scaffolds used as a substrate.

Although the increase of surface electrode area was ~ 340 times, the enhancement in the oxidation peak current density

Fig. 3 Electrochemical characterization of p-BDD electrode in a 0.1 mol L⁻¹ KCl solution. **(a)** CVs at different potential scan rates (10 to 500 mV s⁻¹). Inset represents the linear dependency of the capacitive current on the potential scan rate. **(b)** EIS Bode plot (voltage amplitude = 10 mV) for both types of electrode



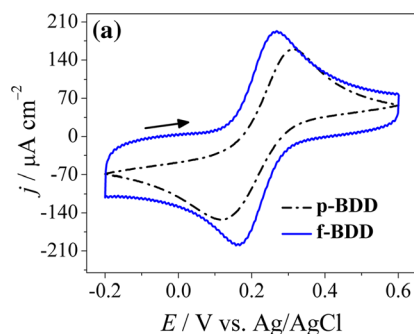
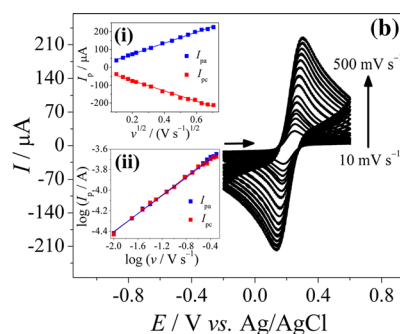


Fig. 4 (a) CVs obtained for a $1.0 \times 10^{-3} \text{ mol L}^{-1} [\text{Fe}(\text{CN})_6]^{3-}$ solution in $0.1 \text{ mol L}^{-1} \text{ KCl}$ using the p-BDD and f-BDD electrodes at $\nu = 50 \text{ mV s}^{-1}$. CVs obtained for a $1.0 \times 10^{-3} \text{ mol L}^{-1} [\text{Fe}(\text{CN})_6]^{3-}$



solution in $0.1 \text{ mol L}^{-1} \text{ KCl}$ using the (b) p-BDD electrode at different potential scan rates ($\nu = 10\text{--}500 \text{ mV s}^{-1}$). Insets—(i) I_p vs. $\nu^{1/2}$ and (ii) $\log I_p$ vs. $\log \nu$

is only ~ 2 times higher for the p-BDD electrode compared to the flat electrode. This might be explained by the limiting rate of diffusion of the redox species to the electrode [34], and experiments to gain a better understanding of this are currently in progress.

Next, we explored the voltammetric response of the two electrodes toward *N,N,N',N'*-tetramethyl-*para*-phenylenediamine (TMPD). TMPD is also a redox probe which undergoes two reversible one-electron oxidation waves [35, 36]. Marker et al. [37, 38] studied the electrochemistry of TMPD on BDD electrodes and found that the response differed depending upon the doping level (i.e. conductivity) of the BDD. They reported a complex voltammetric response for TMPD when a lightly BDD electrode was used [37]. However, a BDD electrode with a higher doping level provided the typical voltammetric response expected for TMPD consisting of two reversible one-electron oxidation waves [38]. This same behaviour was observed using the f-BDD and p-BDD electrodes in the present work.

The CVs obtained for TMPD with our p-BDD and f-BDD electrodes at 50 mV s^{-1} are shown in Fig. 5. As can be seen

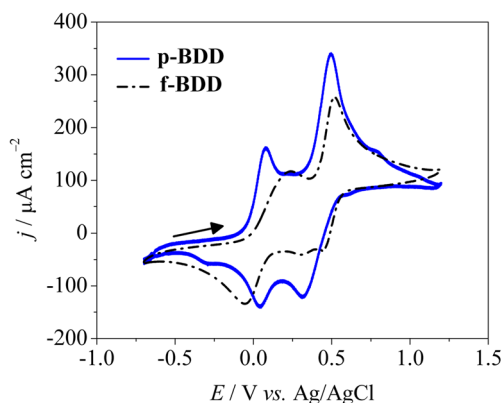


Fig. 5 Cyclic voltammetric profiles of p-BDD (solid line) and f-BDD (dash-dot line) recorded using $1.2 \times 10^{-3} \text{ mol L}^{-1} \text{ TMPD}$ in $0.1 \text{ mol L}^{-1} \text{ KCl}$, $\nu = 50 \text{ mV s}^{-1}$

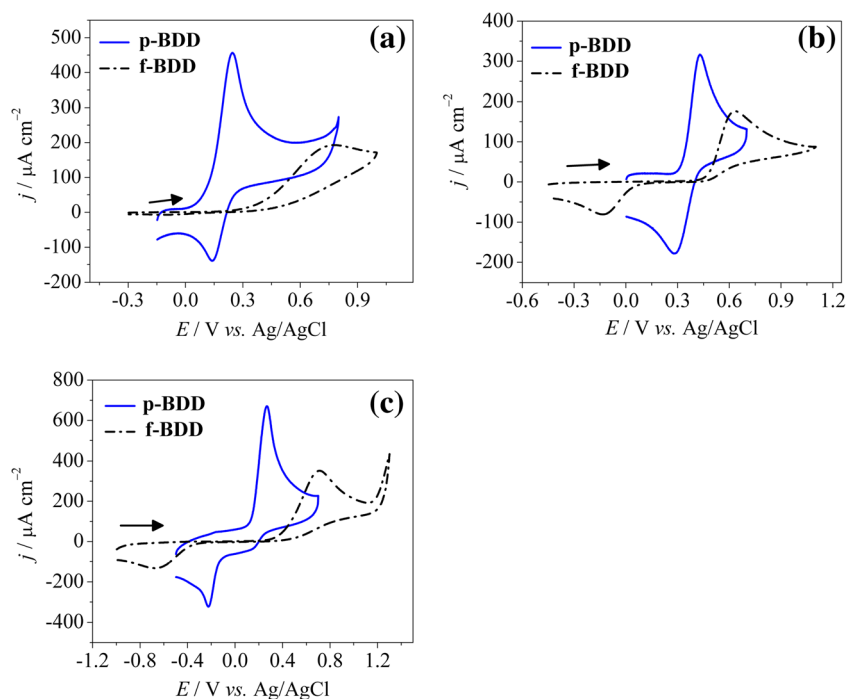
from this figure, the p-BDD electrode presents a higher current density, a cleaner voltammetric profile, and an improvement in electrochemical reversibility for TMPD than the f-BDD electrode. The ΔE_p value obtained for the first redox peak using the f-BDD electrode (293 mV) was about eight times larger than that for the p-BDD electrode (37 mV). Also, the reduction peak for the second redox process was poorly defined for the f-BDD electrode, in contrast to the sharp peak observed with the p-BDD electrode. These results indicate an improved electronic transfer, and a beneficial electrochemical response is apparent at the p-BDD when compared to the conventional f-BDD.

Electrochemical response of biomolecules, DA, AC, and EP on the p-BDD electrode

The electrochemical behaviour of the p-BDD film was investigated for the detection of selected molecules of biological importance. The selected biomolecules were dopamine (DA), epinephrine (EP), and acetaminophen (AC), because these molecules display a well-known electrochemical behaviour and have often been studied electrochemically using carbon-based electrodes [39–42]. Firstly, the CV electrochemical behaviour of these biomolecules was compared using the p-BDD and f-BDD electrodes, with the results shown in Fig. 6.

Figure 6 shows quasi-reversible behaviour for DA and AC and an irreversible profile for EP on p-BDD. However, all biomolecules showed an irreversible behaviour on f-BDD. The p-BDD current densities also were (at least 3 times) higher for all analytes. The decrease in the peak potential with the p-BDD electrode helps improve the sensor selectivity toward competing analytes, while the increase of the analytical signal can improve the sensitivity, limit of detection, and quantification of a chosen analyte. These results for DA, AC, and EP are consistent with the high k^0 values previously obtained for the p-BDD electrode using $[\text{Fe}(\text{CN})_6]^{3-}$. Additionally, the larger current densities on p-BDD are in agreement with our previous work [15].

Fig. 6 CVs obtained for $1.0 \times 10^{-3} \text{ mol L}^{-1}$ DA (a), $1.0 \times 10^{-3} \text{ mol L}^{-1}$ AC (b), and $1.0 \times 10^{-3} \text{ mol L}^{-1}$ EP (c) in 0.2 mol L^{-1} phosphate buffer solution (pH 7.0) using the p-BDD and f-BDD electrodes at $\nu = 50 \text{ mV s}^{-1}$



CV experiments conducted over a large potential scan rate range (10 to 500 mV s^{-1}) explored the electron-transfer process for all three biomolecules on the p-BDD electrode. The I_p values were all close to linear with $\nu^{1/2}$ (data not shown). Plots of $\log I_p$ versus $\log \nu$ were linear with slopes of 0.54 (DA), 0.46 (AC), and 0.42 (EP), which are all close to the expected theoretical value of 0.5 for a diffusion-controlled process [26, 43]. The Nicholson [33] method was selected as a valid method to determine the respective values of k_{app}^0 for DA and AC, because these biomolecules presented a quasi-reversible process controlled by diffusional mass transport. The calculated k_{app}^0 values were $1.3 \times 10^{-3} \text{ cm s}^{-1}$ for DA and $1.8 \times 10^{-3} \text{ cm s}^{-1}$ for AC, assuming a diffusion coefficient for DA of $D = 7.3 \times 10^{-6} \text{ cm}^2 \text{ s}^{-1}$ [44] and for AC of $D = 3.8 \times 10^{-5} \text{ cm}^2 \text{ s}^{-1}$ [45]. These k_{app}^0 values are similar to those found by other authors for DA and AC using a modified CNT paste electrode ($2.21 \times 10^{-3} \text{ cm s}^{-1}$, DA) [44], a porous diamond-like carbon electrode ($5.2 \times 10^{-3} \text{ cm s}^{-1}$, DA, and $4.5 \times 10^{-3} \text{ cm s}^{-1}$, AC) [26] and a graphite electrode ($4.8 \times 10^{-3} \text{ cm s}^{-1}$, DA) [46].

For EP, the analysis was different because the oxidation process on both BDD electrodes was irreversible. Since the process was controlled by diffusional mass transport, the Nicholson-Shain method [47] was now employed to determine k_{app}^0 . The k_{app}^0 values obtained were 1.2×10^{-2} and $4.41 \times 10^{-3} \text{ cm s}^{-1}$ for the p-BDD and the f-BDD electrode, respectively. Thus, the electron-transfer rate constant was almost 3 times higher for p-BDD than for f-BDD, demonstrating the apparent electrocatalytic activity of the BDD surface synthesized

on the VACNT substrate, which contain a high number of carbon nanotube tips (edge planes) exposed.

Conclusions

These results reveal the promising electrochemical performance of porous boron-doped diamond electrodes for use as an electrochemical sensor. The p-BDD material shows electron-transfer rates between 3 and 6 times faster than the conventional flat diamond electrodes extensively used in electroanalysis. Furthermore, the analytical signal magnitude is greatly improved for the p-BDD electrodes, and this can improve sensitivity and electrode performance.

Acknowledgments The authors acknowledge the financial support from the following Brazilian funding agencies: CNPq (561071/2010-1), CAPES and FAPESP (Proc. No. 2014/03019-7 and 2014/02163-7).

References

- Zaidi SA (2013) Int J Electrochem Sci 8(9):11337–11355
- Tan SM, Poh HL, Sofer Z, Pumera M (2013) Analyst 138(17):4885–4891
- Mani V, Chen SM, Lou BS (2013) Int J Electrochem Sci 8(10):11641–11660
- Hupert M, Muck A, Wang R, Stotter J, Cvackova Z, Haymond S, Show Y, Swain GM (2003) Diam Relat Mater 12(10–11):1940–1949
- Pleskov YV (2002) Russ J Electrochem 38(12):1275–1291

6. Peckova K, Musilova J, Barek J (2009) *Crit Rev Anal Chem* 39(3): 148–172
7. Chen MH, Wu GT, Zhu GM, You JK, Lin ZG (2002) *J Solid State Electrochem* 6(6):420–427
8. Tong X, Liu M, Zhao G (2010) *J Solid State Electrochem* 14(2): 221–224
9. Villalba MM, Davis J (2008) *J Solid State Electrochem* 12(10): 1245–1254
10. Luo DB, Wu LZ, Zhi JF (2009) *ACS Nano* 3(8):2121–2128
11. Lv M, Wei M, Rong F, Terashima C, Fujishima A, Gu ZZ (2010) *Electroanalysis* 22(2):199–203
12. Ay A, Swope VM, Swain GM (2008) *J Electrochem Soc* 155(10): B1013–B1022
13. Braga NA, Cairo CAA, Matsushima JT, Baldan MR, Ferreira NG (2010) *J Solid State Electrochem* 14(2):313–321
14. Luo D, Zhi J (2009) *Electrochem Commun* 11(6):1093–1096
15. Zanin H, May PW, Fermin DJ, Plana D, Vieira SMC, Milne WI, Corat EJ (2013) *ACS Appl Mater Interfaces* 6(2):990–995
16. Yang N, Uetsuka H, Williams OA, Osawa E, Tokuda N, Nebel CE (2009) *Phys. Status Solidi A* 206(9):2048–2056
17. Zou Y, May PW, Vieira SMC, Fox NA (2012) *J Appl Phys* 112(4): 044903–044905
18. Gooding JJ (2005) *Electrochim Acta* 50(15):3049–3060
19. Hébert C, Mazellier JP, Scorsone E, Mermoux M, Bergonzo P (2014) *Carbon* 71(0):27–33
20. Gao F, Wolfer MT, Nebel CE (2014) *Carbon* 80(0):833–840
21. Yang N, Smirnov W, Nebel CE (2013) *Electrochem Commun* 27(0):89–91
22. Kato H, Hees J, Hoffmann R, Wolfer M, Yang N, Yamasaki S, Nebel CE (2013) *Electrochem Commun* 33(0):88–91
23. Zanin H, May PW, Hamiman RL, Risbridger T, Corat EJ, Fermin DJ (2015) *Carbon* 82(0):288–296
24. Silva TA, Zanin H, Saito E, Medeiros RA, Vicentini FC, Corat EJ, Fatibello-Filho O (2014) *Electrochim Acta* 119(0):114–119
25. Fox OJ, Holloway JO, Fuge GM, May PW, Ashfold MN (2009) *Electrospray deposition of diamond nanoparticle nucleation layers for subsequent CVD diamond growth* (2009) *MRS Proceedings* (1203):J17–27
26. Silva TA, Zanin H, May PW, Corat EJ, Fatibello-Filho O (2014) *ACS Appl Mater Interfaces* 6(23):21086–21092
27. Brett CMA, Brett AMO (1993) *Electrochemistry: principles, methods, and applications*. Oxford Science Publications, Oxford
28. Swain GM (1994) *Adv Mater* 6(5):388–392
29. Swain GM, Ramesham R (1993) *Anal Chem* 65(4):345–351
30. Brownson DAC, Kampouris DK, Banks CE (2012) *Chem Soc Rev* 41(21):6944–6976
31. Chen PH, Fryling MA, McCreery RL (1995) *Anal Chem* 67(18): 3115–3122
32. Kneten KR, McCreery RL (1992) *Anal Chem* 64(21):2518–2524
33. Nicholson RS (1965) *Anal Chem* 37(11):1351
34. Smirnov W, Kriele A, Yang N, Nebel CE (2010) *Diam Relat Mater* 19(2–3):186–189
35. Schroder U, Wadhawan JD, Compton RG, Marken F, Suarez PAZ, Consorti CS, de Souza RF, Dupont J (2000) *New J Chem* 24(12): 1009–1015
36. Evans RG, Klymenko OV, Hardacre C, Seddon KR, Compton RG (2003) *J Electroanal Chem* 556(0):179–188
37. Marken F, Compton GR, Goeting HC, Foord SJ, Bull DS, Davies GS *J Solid State Electrochem* 5 (2):88–93
38. Hyde M, Saterlay AJ, Wilkins SJ, Foord JS, Compton RG, Marken F (2014) *J Solid State Electrochem* 6(3):183–187
39. Tsierkezos NG, Ritter U (2012) *J Solid State Electrochem* 16(6): 2217–2226
40. Yang H, Li Y, Liu Y, Zhang Y, Zhao Y, Zhao M (2014) *J Solid State Electrochem* 19(1):145–152
41. Raouf JB, Chekin F, Ojani R, Barari S, Anbia M, Mandegarad S (2012) *J Solid State Electrochem* 16(12):3753–3760
42. Houshmand M, Jabbari A, Heli H, Hajjizadeh M, Moosavi-Movahedi AA (2007) *J Solid State Electrochem* 12(9):1117–1128
43. Bard AJ, Faulkner LR (2000) *Electrochemical methods: fundamentals and application*, 2nd ed. John Wiley & Sons, New York
44. Mazloum-Ardakani M, Beitollahi H, Ganjipour B, Naeimi H, Nejati M (2009) *Bioelectrochemistry* 75(1):1–8
45. Wang CH, Li CY, Wang F, Wang CF (2006) *Microchim Acta* 155(3–4):365–371
46. Li Q, Wang Y, Luo G (2000) *Mater Sci Eng C* 11(1):71–74
47. Nicholson RS, Shain I (1964) *Anal Chem* 36(4):706–723